Single Phase Bidirectional H6 Rectifier/Inverter

Jianhua Wang, *Member, IEEE*, Shang Gao, Yichao Sun, *Member, IEEE*, Zhendong Ji, Lexiang Cheng, Lingyu Li, Wei Gu, *Senior Member, IEEE*, and Jianfeng Zhao

***Abstract*—Transformerless photovoltaic (PV) inverters are more widely adopted due to high efficiency, low cost, light weight, etc. However, H5, HERIC, etc., transformerless PV inverters do not have the bidirectional capability for a solar energy storage system in the future. With topology derivation history reviewed from rectifier to inverter, the essence of bidirectional rectifier/inverter is revealed to find a reverse power flow approach. Therefore, this paper proposes an advanced bidirectional technique for a selected H6 inverter topology with only a modulation strategy modified, while the others remain the same. For the H6 circuitry in both rectifier and inverter modes, an excellent three level DM voltage feature is achieved, while leakage current issue is eliminated at the same time with improved modulation method. Simulations and experimental results verify the proposed single phase bidirectional H6 rectifier/inverter technique.**

***Index Terms*—Bidirectional power flow, H6 inverter, improved modulation, leakage current, rectifier.**

I. Introduction

HIGH penetration installed renewable energies are playing more important roles in the electric power system, which gradually change the existing utility grid with more power electronics features due to grid-connected converters [1]. In summer weekends, renewable energies already provide 100% of demand in Germany [2]. The fundamental operation codes for the existing power grid are continuously modified for grid-tie inverters, especially for PV applications [3]. The grid codes are not only focusing on unilateral restrictions on leakage current safety, harmonic limits, and anti-islanding requirements, but also place

Manuscript received August 21, 2018; revised November 26, 2018; accepted January 26, 2019. Date of publication February 7, 2019; date of current version August 29, 2019. This work was supported in part by the Natural Science Foundation of Jiangsu Province (BK20181283), in part by the Science and Technology Project of State Grid Jiangsu Electric Power Co. Ltd of China (J2018081), and in part by the Fundamental Research Funds for the Central Universities (2242018K41066). Recommended for publication by Associate Editor T. Shimizu. *(Corresponding author: Jianhua Wang.)*

J. Wang, S. Gao, W. Gu, and J. Zhao are with the Jiangsu Provincial Key Laboratory of Smart Grid Technology & Equipment, School of Electrical Engineering, Southeast University, Nanjing 210096, China (e-mail:

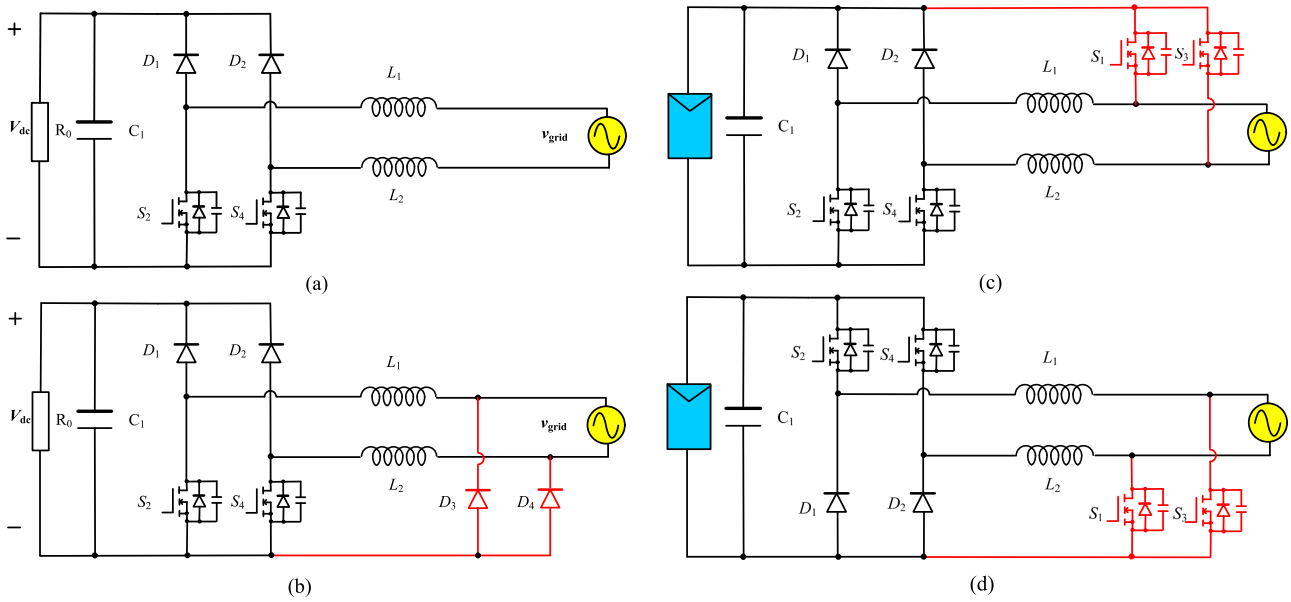

Fig. 1. Relationship between bridgeless PFC boost rectifier and transformerless inverter. (a) Basic bridgeless PFC boost rectifier. (b) Improved bridgeless PFC boost rectifier. (c) Transformerless inverter with open emitter in the high side. (d) Improved transformerless inverter with open emitter in the low side.

leakage currents can be minimized in the proposed topology both in inversion and rectification modes. Based on the high-frequency leg technique, Liu *et al.* [21] further improves the dual buck-type full bridge bidirectional ac–dc converter with discontinuous current mode/continuous current mode operations.

For full-bridge type inverter, classic H5, HERIC, etc. transformerless PV inverters do not have the bidirectional capability [21]. However, these topologies and derived circuitries such as numerous H6 inverters are the dominant circuits in single phase transformerless PV applications. Since bidirectional power capability is a challenge to existing H6 inverters, the motivation of this manuscript is to find an advanced solution for them. In this paper, the relationship between bridgeless PFC boost rectifier and the transformerless inverter is reviewed and expounded at first. Then, a novel modulation method is proposed for a single phase H6 inverter reform. It not only has an bidirectional power flow feature but also retains the existing H6 inverter advantages, e.g., CM voltage and high efficiency. At last, PSIM simulations and experimental test results verify the proposed single phase bidirectional H6 rectifier/inverter.

II. Relationship Between Bridgeless PFC Boost Rectifier and Transformerless Inverter

In most cases, the boost topology is used for single-phase active power factor correction with input diode rectifier. The current has to pass at least three semiconductors including two diodes. Classic bridgeless PFC boost rectifier using split chokes without the input rectifier for each half-wave in Fig. 1(a) is proposed. The problem is that the connection of both input lines to a PFC choke. The outcome of this is the floating of the output with high frequency relative to the input source.

A new topology invented by Ernö and Frisch in Vincotech does solve the problem [22]. Two chokes with the same inductance as in the standard boost topology are required. But only one inductor is used per half wave. The other one is bypassed by additional rectifiers as illustrated in Fig. 1(b). It is interesting to find that four years later Frisch and Ernö also proposed transformerless inverter with the open emitter in the high side in Fig. 1(c), which is switched only with 50 Hz as D_3, D_4 in Fig. 1(b) [23].

Similarly, another transformerless inverter with the open emitter in the low side is proposed in [24] as illustrated in Fig. 1(d). The basic idea behind it is to associate two parallel step-down converters with the output connected to the load using the opposite polarities. It is derived from [25], where one of the discussed power-factor correction circuits was modified to get a reverse power flow.

In general, Fig. 1 summarizes the relationship between bridgeless PFC boost rectifier and transformerless inverter, the essence of variant circuits is to find a reverse power flow approach, which would help bidirectional rectifier/inverter developed.

III. Selected H6 Inverter With a Reverse Power Flow

A. Selected H6 Inverter With Its Corresponding Hybrid Modulation Method

H5, HERIC, and H6 types are the dominant topologies in single phase transformerless PV inverters. One H6 inverter as shown in Fig. 2 is selected as an example for further analysis below. Fig. 3 further illustrates its corresponding hybrid modulation method for the selected H6 inverter, where intermediate active devices S_5 and S_6 are switched only with line frequency 50/60 Hz. The diagonal active devices S_1, S_4, and S_2, S_3 are high-frequency switches during a positive grid cycle or a nega-

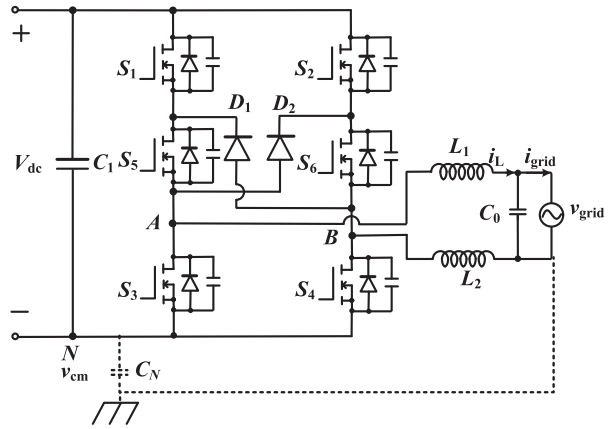

Fig. 2. Selected H6 inverter.

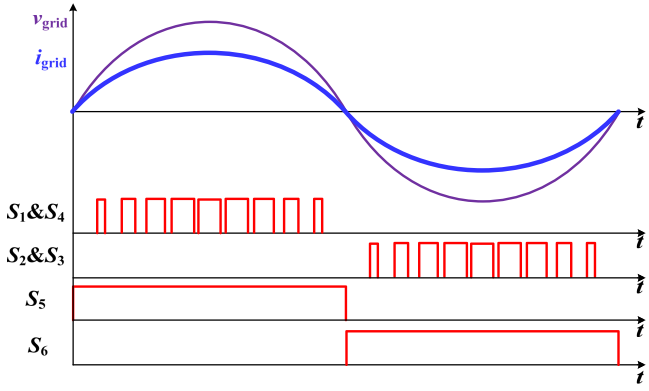

Fig. 3. Corresponding hybrid modulation method for the selected H6 inverter.

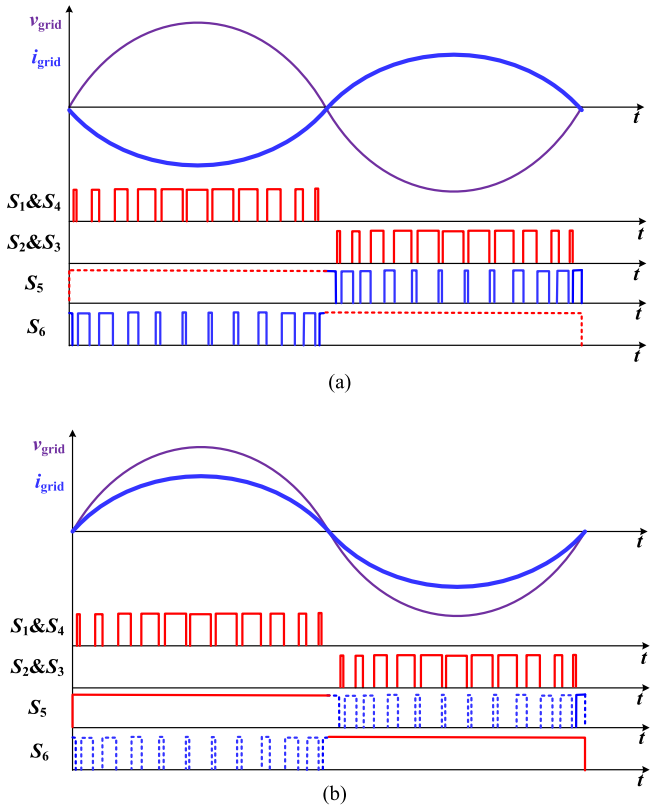

Fig. 4. Novel hybrid modulation method for selected H6 converter. (a) Rectifier modulation mode. (b) Inverter modulation mode.

tive grid cycle, respectively. Most of the existing literature about H6 topologies only covers grid-connected applications.

B. Bidirectional H6 Rectifier/Inverter With Novel Hybrid Modulation Method

Focusing on energy storage application in the near future, a novel hybrid modulation method is proposed in Fig. 4 for the selected bidirectional H6 converter in Fig. 2. Fig. 4(a) and (b) shows the rectifier and inverter modulation modes, respectively. It is found that the high frequency switching patterns for S_1, S_4, and S_2, S_3 remains the same. During former OFF mode in Fig. 3, line frequency switches S_5, S_6 in Fig. 4 also switch with high-frequency pulses, which are the opposite of S_1, S_4, and S_2, S_3, respectively.

It should be noted that the added high-frequency pulses for S_5, S_6 are invalid for H6 inverter as illustrated in Fig. 4(b). With additional drive signals applied, the voltages, currents, and power flows remain the same as that in Fig. 3. Detail operation modes and analysis for Fig. 4 are presented in the next Section III-C.

C. Bidirectional H6 Rectifier/Inverter Operation Modes

In H6 rectifier mode 1, as shown in Fig. 5(a), during positive grid cycle while S_5 is always ON, S_6 is turned ON with high frequency, and grid charges the chokes L_1 and L_2 through a combination of the path between grid, L_1, D_2, S_6, and L_2.

Although S_5 is ON, no current flow through it. However, with the contribution of shorten S_5, $v_{\rm AN} = 0.5\ V_{\rm dc}$ due to split voltage between deactivated S_1 and S_3. For the same reason, $v_{\rm BN} = 0.5\ V_{\rm dc}$, therefore,

$$\begin{aligned}&\text{Differential mode voltage } v_{\rm dm} = v_{\rm AB} = v_{\rm AN} - v_{\rm BN} = 0\\ &\text{Differential mode voltage } v_{\rm cm} = (v_{\rm AN} + v_{\rm BN})/2 = 0.5\ V_{\rm dc}.\end{aligned} \tag{1}$$

In H6 rectifier mode 2, as shown in Fig. 5(b), during a positive grid cycle while S_5 is always ON, S_6 is turned OFF with high frequency. With active S_1 and S_4, continuous inductor current finds the demagnetization path for chokes L_1 and L_2: grid, L_1, D_2, D_{S2}, dc side, $S_4(D_{S4})$, and L_2, which is a reverse inner path for bidirectional power flow.

Since S_1 and S_5 are turned ON, bridge middle-point A is clamped to dc bus high side, then $v_{\rm AN} = V_{\rm dc}$. At the same time, bridge middle-point B is clamped to dc bus low side, therefore, $v_{\rm BN} = 0$

$$\begin{aligned}v_{\rm dm} &= v_{\rm AB} = v_{\rm AN} - v_{\rm BN} = V_{\rm dc}\\ v_{\rm cm} &= (v_{\rm AN} + v_{\rm BN})/2 = 0.5\ V_{\rm dc}.\end{aligned} \tag{2}$$

In H6 rectifier mode 3, as shown in Fig. 5(c), during a negative grid cycle while S_6 is always ON, S_6 is turned ON with high frequency, and it is a mirror state as illustrated in mode 1.

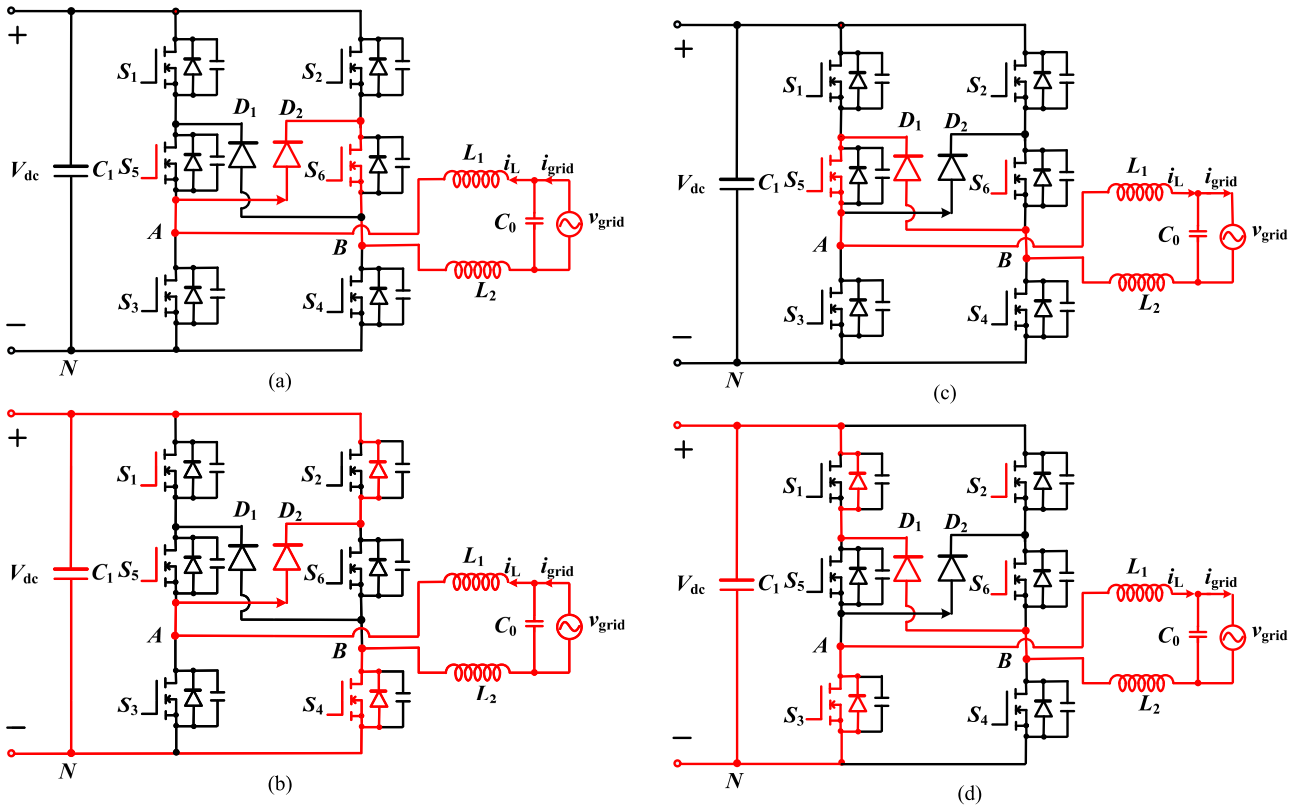

Fig. 5. H6 rectifier operation modes. (a) Mode 1. (b) Mode 2. (c) Mode 3. (d) Mode 4.

The reverse power flow loop is a combination of the path between grid, L_2, D_1, S_5, and L_1. Similarly

$$v_{\rm dm} = v_{\rm AB} = v_{\rm AN} - v_{\rm BN} = 0.5\ V_{\rm dc} - 0.5\ V_{\rm dc} = 0$$
$$v_{\rm cm} = (v_{\rm AN} + v_{\rm BN})/2 = (0.5\ V_{\rm dc} + 0.5\ V_{\rm dc})/2 = 0.5\ V_{\rm dc}. \quad (3)$$

In H6 rectifier mode 4, as shown in Fig. 5(d), during a negative grid cycle while S_6 is always ON, S_5 is turned OFF with high frequency, and it is a mirror state as illustrated in mode 2. Power flow loop is a combination of path between grid, L_2, D_1, D_{S1}, dc side, $S_3(D_{S3})$, and L_2. Similarly

$$v_{\rm dm} = v_{\rm AB} = v_{\rm AN} - v_{\rm BN} = 0 - V_{\rm dc} = -V_{\rm dc}$$
$$v_{\rm cm} = (v_{\rm AN} + v_{\rm BN})/2 = (0 + V_{\rm dc})/2 = 0.5\ V_{\rm dc}. \quad (4)$$

Fig. 6 also presents H6 inverter operations modes following modulation mode in Fig. 4, detail operations are provided below.

In H6 inverter mode 1, as shown in Fig. 6(a), during a positive grid cycle while S_5 is always ON, S_1 and S_4 are turned ON synchronously with same high frequency, and dc side charges the chokes L_1, L_2, and grid through a combination of path between S_1, S_5, L_1, grid, L_2, S_4.

Since S_1 and S_5 are turned on, bridge middle-point A is-clamped to dc bus high side, then $v_{\rm AN} = V_{\rm dc}$. At the same time, bridge middle-point B is clamped to dc bus low side, therefore, $v_{\rm BN} = 0$

Differential mode voltage $v_{\rm dm} = v_{\rm AB} = v_{\rm AN} - v_{\rm BN} = V_{\rm dc}$

Common mode voltage $v_{\rm cm} = (v_{\rm AN} + v_{\rm BN})/2 = 0.5\ V_{\rm dc}$. (5)

In H6 inverter mode 2, as shown in Fig. 6(a), during a positive grid cycle while S_5 is always ON. With deactivated S_1 and S_4, continuous inductor current finds the freewheeling path for chokes L_1 and L_2: grid, L_2, D_1, S_5, and L_2.

Although S_6 is turned ON with high frequency at this time, no current flow through it. However, with the contribution of shorten S_6, $v_{\rm BN} = 0.5\ V_{\rm dc}$ due to split voltage between deactivated S_2 and S_4. For the same reason, $v_{\rm AN} = 0.5\ V_{\rm dc}$, therefore

$$v_{\rm dm} = v_{\rm AB} = v_{\rm AN} - v_{\rm BN} = 0$$
$$v_{\rm cm} = (v_{\rm AN} + v_{\rm BN})/2 = 0.5\ V_{\rm dc}. \quad (6)$$

In H6 inverter mode 3, as shown in Fig. 6(c), during a negative grid cycle while S_6 is always ON, S_2 and S_3 are turned ON with the high frequency, and it is a mirror state as illustrated in mode 1. The power flow loop is a combination of the path between grid, L_1, S_3, dc side, S_2, S_6, and L_2. Similarly

$$v_{\rm dm} = v_{\rm AB} = v_{\rm AN} - v_{\rm BN} = 0 - V_{\rm dc} = -V_{\rm dc}$$
$$v_{\rm cm} = (v_{\rm AN} + v_{\rm BN})/2 = (0 + V_{\rm dc})/2 = 0.5\ V_{\rm dc}. \quad (7)$$

In H6 inverter mode 4, as shown in Fig. 6(d), during a negative grid cycle while S_6 is always ON, S_5 is turned ON with high frequency, and it is a mirror state as illustrated in mode 2.

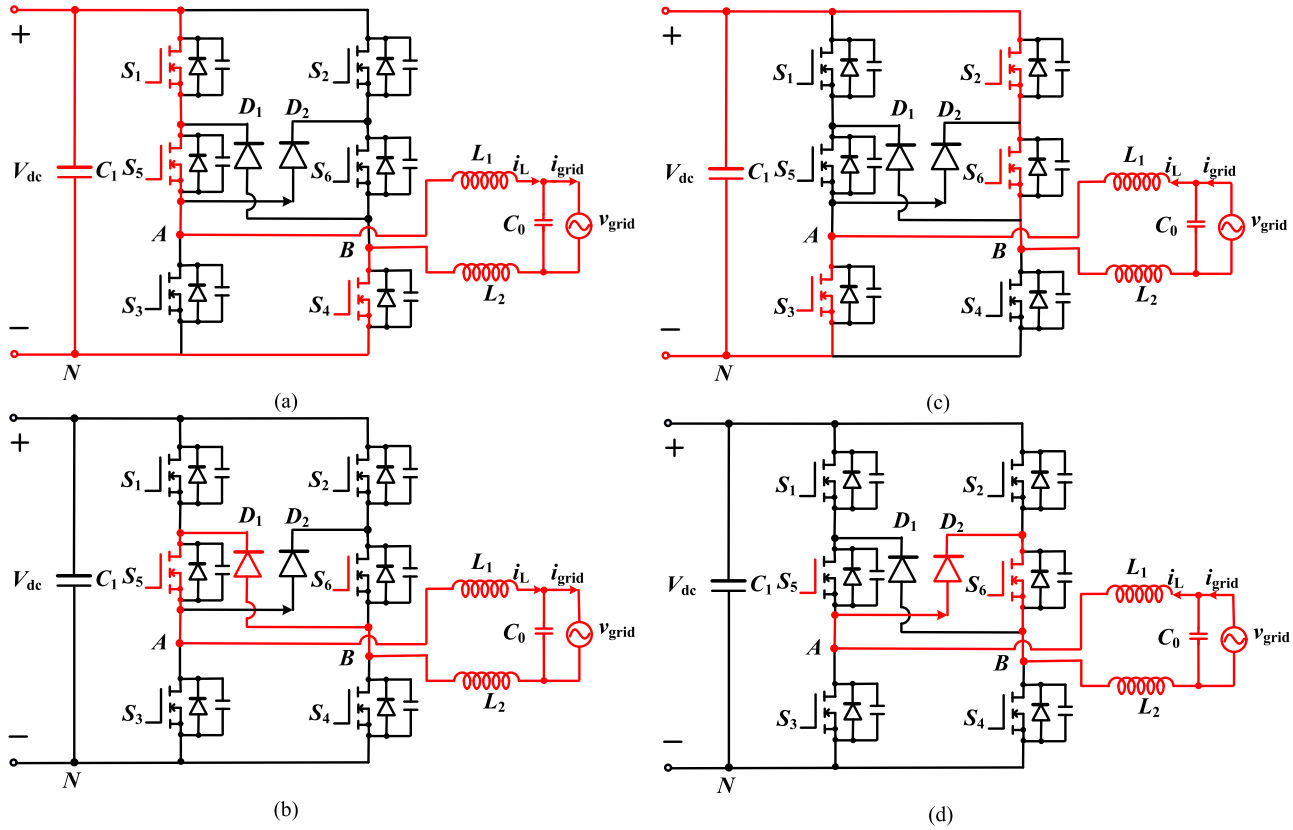

Fig. 6. H6 inverter operation modes. (a) Mode 1. (b) Mode 2. (c) Mode 3. (d) Mode 4.

Current Freewheeling loop is a combination of the path between grid, L_2, D_1, S_3, and L_1. Similarly

$$v_{\rm dm} = v_{\rm AB} = v_{\rm AN} - v_{\rm BN} = 0.5\ V_{\rm dc} - 0.5\ V_{\rm dc} = 0$$
$$v_{\rm cm} = (v_{\rm AN} + v_{\rm BN})/2 = (0.5\ V_{\rm dc} + 0.5\ V_{\rm dc})/2 = 0.5\ V_{\rm dc}. \quad (8)$$

IV. Discussion and Design Consideration

A. Advanced DM, CM Features for Bidirectional H6 Converter With Proposed Modulation Method

With detail operation modes analyzed in Section III, Table I further summarizes some important features for the bidirectional H6 inverter. It is found that no matter it is a rectifier or inverter, CM voltage of the bidirectional H6 inverter is almost a constant dc value, which would eliminate inverter's leakage current and improve EMC characteristic of PFC converter.

On the other hand, the differential voltage changes between $V_{\rm dc}$, 0, and $-V_{\rm dc}$. It is a typical three-level voltage, which indicates good power quality of the grid side, no matter it is a rectifier or inverter.

TABLE I
Comparison Summary

Figures	Traditional Hybrid Modulation Method	Improved Hybrid Modulation Method	Corresponding Current paths	Level	
				$v_{\rm cm}$	$v_{\rm dm}$
Figure 5(a)	/	Rectifier Mode 1	grid, L_1, D_2, S_6, and L_2	0.5$V_{\rm dc}$	0
Figure 5(b)	/	Rectifier Mode 2	grid, L_1, D_2, D_{S2}, dc side, S_4 (D_{S4}), and L_2	0.5$V_{\rm dc}$	$V_{\rm dc}$
Figure 5(c)	/	Rectifier Mode 3	grid, L_2, D_1, S_5, and L_1	0.5$V_{\rm dc}$	0
Figure 5(d)	/	Rectifier Mode 4	grid, L_2, D_1, D_{S1}, dc side, S_3 (D_{S3}), and L_1	0.5$V_{\rm dc}$	-$V_{\rm dc}$
Figure 6(a)	Inverter Mode 1	Inverter Mode 1	S_1, S_5, L_1, grid, L_2, and S_4	0.5$V_{\rm dc}$	$V_{\rm dc}$
Figure 6(b)	Inverter Mode 2	Inverter Mode 2	grid, L_2, D_1, S_5, and L_1	0.5$V_{\rm dc}$	0
Figure 6(c)	Inverter Mode 3	Inverter Mode 3	grid, L_1, S_3, dc side, S_2, S_6, and L_2	0.5$V_{\rm dc}$	-$V_{\rm dc}$
Figure 6(d)	Inverter Mode 4	Inverter Mode 4	grid, L_2, D_1, S_3, and L_1	0.5$V_{\rm dc}$	0

B. Modulation Comparison for Bidirectional Power Flow and Unidirectional Power Flow

In Table I, it is found that H6 inverter operation modes with the proposed modulation strategy or traditional modulation method are almost the same. The differences are high frequency switching patterns for with S_5 and S_6 with a dashed line in Fig. 4(b). Actually, the dashed switching pulses could also be removed for inverter mode. For the same reason, line frequency switching pulses for with S_5 and S_6 with dashed line could also be removed for rectifier mode as Fig. 4(a). In this way, modulation strategies for both modes are different and should be changed with mode

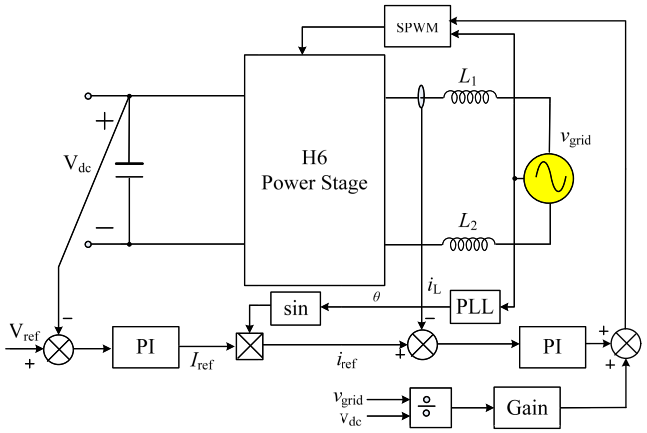

Fig. 7. Control block of the H6 converter with bidirectional power flow.

transfer. For control simplicity, we choose the same modulation method including some redundancy switching signals.

On the other hand, differences between Fig. 4(a) and (b) are that high frequency switching pulses adopted in S_5 and S_6 for rectifier mode, while line frequency switching pulses adopted in S_5 and S_6 for inverter mode. Corresponding current paths in Table I further illustrate that body diodes are used in rectifier mode while they are not adopted in inverter mode. These two would affect the efficiency of the rectifier mode, which is the inevitable cost with only concise modulation improvement adopted. Fortunately, a single H6 inverter solution is suitable for small power fields, where battery storage is adopted for emergency usage. The slight efficiency decrease is acceptable for practice.

C. Bidirectional H6 Rectifier/Inverter Control Method

Fig. 7 shows the control block of the bidirectional H6 converter. The HV bus voltage $V_{\rm dc}$ is regulated by the dc bus feedforward voltage loop control. The output current magnitude $I_{\rm ref}$ is given by the voltage loop. The instantaneous current reference value $i_{\rm ref}$ is obtained by $I_{\rm ref}$ multiplied by a sine table which is synchronous with the grid voltage through PLL circuit. A fast current inner loop guarantees the inductor current tracks the reference current value $i_{\rm ref}$, where grid voltage and dc bus voltage are used with a divider. Finally, the SPWM signals generation block is set as shown in Fig. 4.

V. Simulation and Experimental Verification

In order to verify the proposed hybrid modulation method for the H6 bidirectional converter, PSIM simulations and experimental test results are provided for verification, respectively. Main related parameters of the H6 schematic are listed in Table II, respectively.

A. Simulation Results

Fig. 8 provides detail simulation results for H6 rectifier mode and inverter mode verification, including ac grid voltage, ac current, DM voltage, CM voltage, and drive signals, which are predicted in Section III.

TABLE II
Main Parameters of the Converter

Parameter	Value
DC bus voltage	V_{dc}=380 VDC
Grid voltage	v_{grid}=220 VAC/50 Hz
Switching frequency	f_s =20 kHz
Output inductors	$L_1 = L_2$= 500 μH
Output capacitor	C_{out}=4.7 μF

Fig. 9 further provides current stress and voltage stress of the main device in the H6 rectifier. Due to the symmetrical structure of the circuit, D_1, S_1, S_3, S_5 are chosen for device selection. It is found that the transient maximum current of them is given by the inductor current with high-frequency ripple considered. While the transient maximum voltage of them is clamped to the dc link voltage. Considering the thermal issue and voltage spike, 1.5 × –2 × current/voltage derating coefficient would be acceptable.

B. Experimental Test Results

Fig. 10 further shows the 5-kW bidirectional prototype photograph based on H6-typer topology. Detail test results are provided below.

Fig. 11(a) shows that the ac current is of the opposite phase from the ac current, while ac current and ac voltage in Fig. 11(b) maintain the same frequency, as well as phase. The two curves are typical rectifier and inverter waveform with power factor $= -1$, and 1, respectively. Double line frequency dc link voltage ripple is also observed in Fig. 11, it is a typical single phase system feature. The grid current total harmonic distortion of the rectifier mode and inverter mode is 3.28% and 2.64%, respectively, which both indicate high grid current performance. However, it is found that there are still small distortions in zero-crossing points. There are many reasons for zero crossing distortion, e. g. reactive power, dead time, discontinues inductor current mode, modulation methods, impedance with nonideal loop gain, etc. And the zero-crossing distortion could be eliminated following the way of [26]–[29] in the future.

Figs. 12 and 13 illustrate detail gate signals of each active switch. It is found that no matter the converter is a rectifier or inverter, the switching pattern is the same, which implies that the same PWM modulation method is adopted as Fig. 4 illustrates.

Fig. 14 provides DM voltage and 2 × CM voltage of the bidirectional H6 converter. Typical $+1, 0, -1$ three level voltage shows its DM voltage advantage, while constant dc voltage with small ac ripple verifies excellent CM voltage and leakage current feature as illustrated in Fig. 8.

Last but not the least, the efficiency curve of both rectifier mode and inverter mode are shown in Fig. 15. It is found that the maximum efficiency of the converter in inversion mode is 96.95%, while that in rectifier mode is 96.24% in rectification mode. In rectifier mode, switching two switches with high frequency and using body diodes for power flow paths will definitely increase the switching losses of the converter, compared

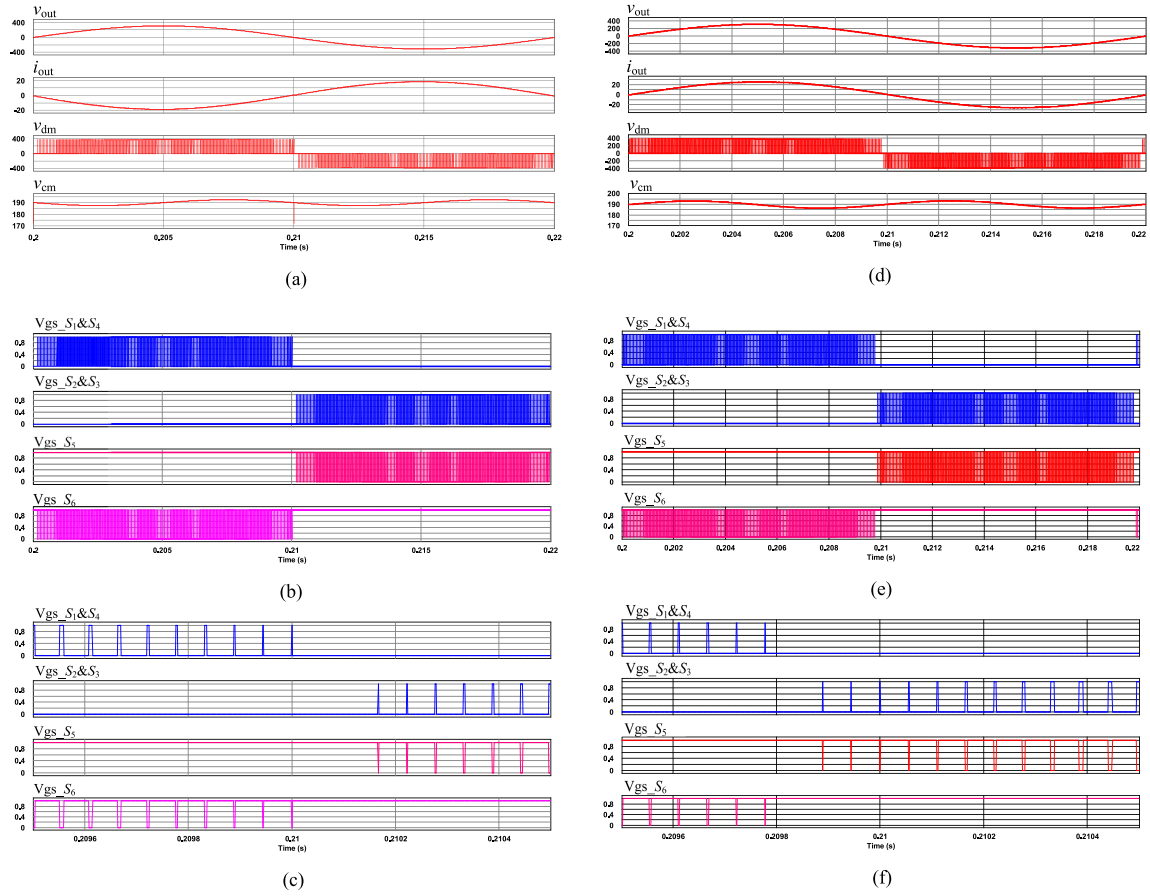

Fig. 8. Bidirectional H6 rectifier/inverter modulation method simulation results. (a) AC grid voltage, ac current, DM voltage, and CM voltage in rectifier mode. (b) Switching pulses S_1 and S_4, S_2 and S_3, S_5, S_6 in rectifier mode. (c) Expanded switching pulses S_1 and S_4, S_2 and S_3, S_5, S_6 in rectifier mode. (d) AC grid voltage, ac current, DM voltage, and CM voltage in inverter mode. (e) Switching pulses S_1 and S_4, S_2 and S_3, S_5, S_6 in inverter mode. (f) Expanded switching pulses S_1 and S_4, S_2 and S_3, S_5, S_6 in inverter mode.

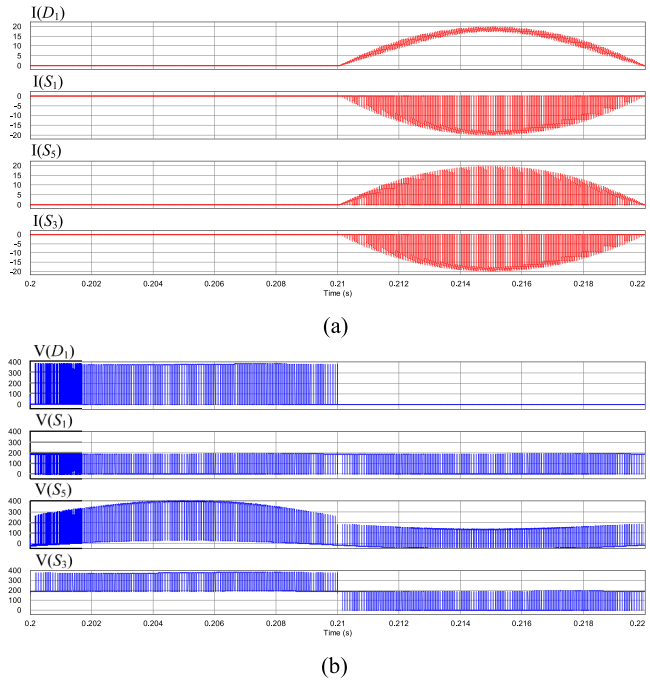

Fig. 9. H6 rectifier device stress. (a) Current stress. (b) Voltage stress.

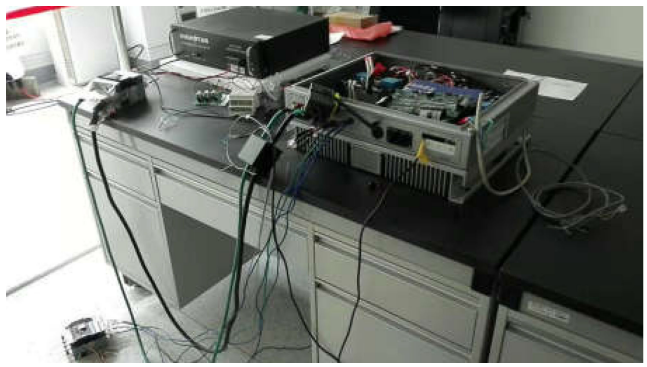

Fig. 10. Prototype photograph.

to the H6 inverter mode. It is the cost for bidirectional power capability like that in the bi-polar modulation method and uni-polar modulation method for full bridge inverter. The efficiency of the H6 rectifier slights lower that H6 inverter.

The most known bidirectional converter is the bi-polar modulation single phase full bridge H4 converter. It is proven that the H6-type converter is more efficient than the bi-polar modulation H4 inverter due to body diode is replaced with an extra independent diode at the cost of more devices. Following this way,

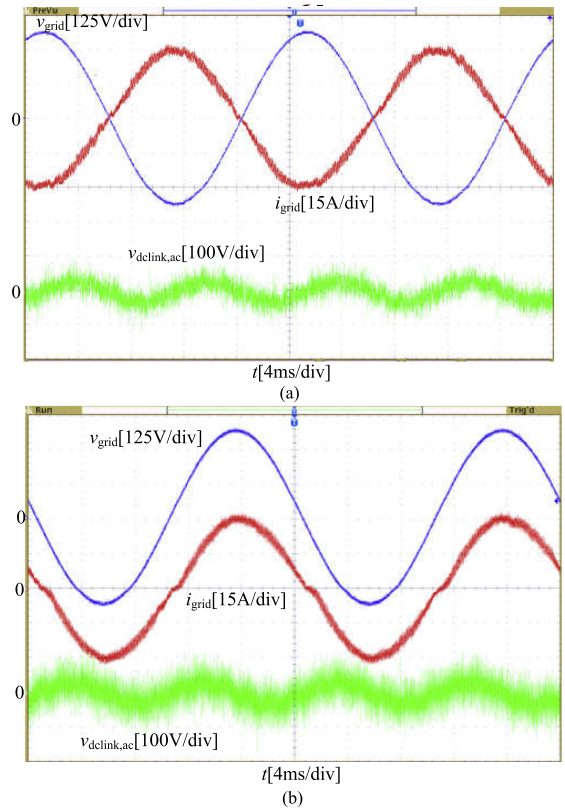

Fig. 11. AC grid voltage, ac current, and dc link voltage ac ripple. (a) H6 rectifier mode. (b) H6 inverter mode.

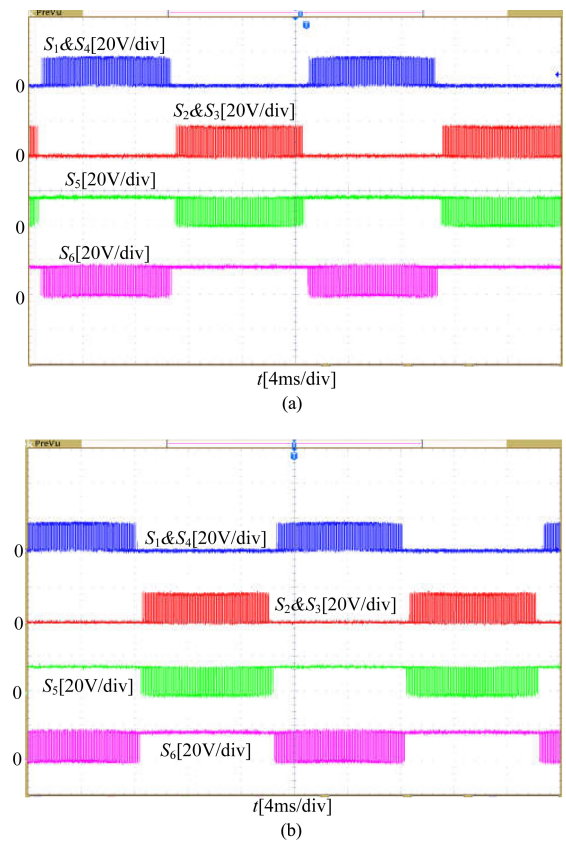

Fig. 12. Switching pulses. (a) H6 rectifier mode. (b) H6 inverter mode.

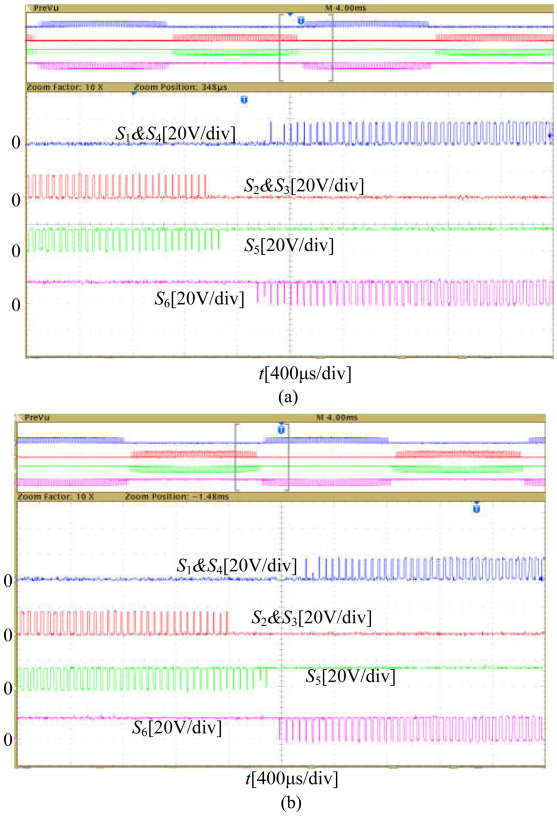

Fig. 13. Expanded switching pulses. (a) H6 rectifier mode. (b) H6 inverter mode.

cost performance concern.

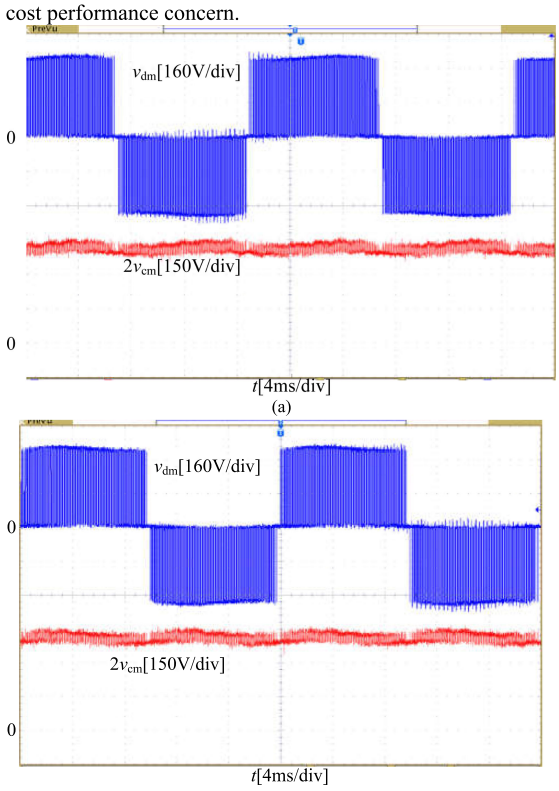

Fig. 14. CM voltage, DM voltage (2 × CM voltage $2v_{\rm cm} = v_{\rm AN} + v_{\rm BN}$ measured with oscilloscope math function). (a) H6 rectifier mode. (b) H6 inverter mode.

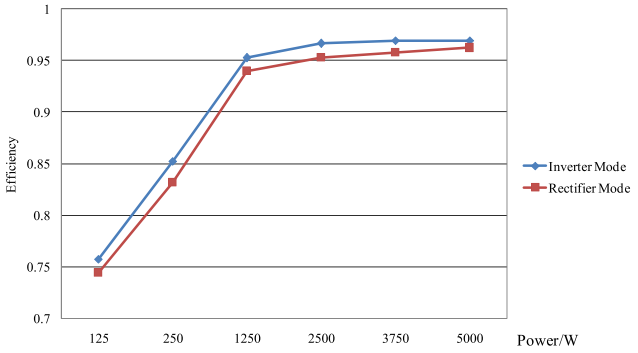

Fig. 15. Efficiency curve.

with more active and passive devices enrolled, dual buck-type converter, three-level converters and their derived converters would get more high efficiency but the circuit structures would be more complex. Therefore, considering H6-type converters are the dominant circuits in single phase transformerless PV applications, the proposed methodology would be regarded as a good tradeoff for high-cost performance concern.

VII. Conclusion

Aiming solar energy storage system, this paper improves a grid-tied single phase H6 PV inverter from unidirectional power flow to bidirectional power flow. A unified hybrid modulation method is proposed for both rectifier and inverter modes. The main advantages of the proposed solution can be summarized as follows.

1) Compared with the traditional hybrid modulation method for power rejection to the grid only, a simple modification in the switching patterns is just needed for a solar energy storage system with H6 type topology.
2) Battery storage is adopted for emergency usage in a small solar energy storage system. Therefore, a slight cost of efficiency decreases in rectifier mode due to the partly used body diodes is acceptable, and the excellent DM/CM voltage features of the H6 circuitry in both rectifier and inverter modes are totally achieved.
3) The improved hybrid modulation method would be easily modified and applied to other H6 and similar topologies.

Acknowledgment

The authors would like to thanks Dr. M. Luo from Plexim GmbH for his kind instruction and help in PLECS RT Box HIL Platform for Power Electronics, which significantly improve their verification work.

References

[1] R. Teodorescu, M. Liserre, and P. Rodriguez, *Grid Converters for Photovoltaic and Wind Power Systems*. Hoboken, NJ, USA: Wiley, 2011.
[2] R. W. De Doncker, "Power electronics—Key enabling technology for a CO_2 neutral electrical energy supply," 2017. [Online]. Available: http://www.ifeec.tw/ee2017/keynote.html
[3] Generators connected to the low-voltage distribution network. Available at: https://www.vde-verlag.de/standards/0105029/vde-ar-n-4105-anwendungsregel-2011-08.html
[4] T. Kerekes, R. Teodorescu, P. Rodriguez, G. Vazquez, and E. Aldabas, "A new high-efficiency single-phase transformerless PV inverter topology," *IEEE Trans. Ind. Electron.*, vol. 58, no. 1, pp. 184–191, Jan. 2011.
[5] R. Bojoi, L. R. Limongi, D. Roiu, and A. Tenconi, "Enhanced power quality control strategy for single-phase inverters in distributed generation systems," *IEEE Trans. Power Electron.*, vol. 26, no. 3, pp. 798–806, Mar. 2011.
[6] M. Yilmaz and P. T. Krein, "Review of the impact of vehicle-to-grid technologies on distribution systems and utility interfaces," *IEEE Trans. Power Electron.*, vol. 28, no. 12, pp. 5673–5689, Dec. 2013.
[7] B. Ji, J. Wang, and J. Zhao, "High-efficiency single-phase transformerless PV H6 inverter with hybrid modulation method," *IEEE Trans. Ind. Electron.* vol. 60, no. 5, pp. 2104–2115, May 2013.
[8] L. Zhang, K. Sun, L. Feng, H. Wu, and Y. Xing, "A family of neutral point clamped full-bridge topologies for transformerless photovoltaic grid-tied inverters," *IEEE Trans. Power Electron.*, vol. 28, no. 2, pp. 730–739, Feb. 2013.
[9] W. Li *et al.*, "Topology review and derivation methodology of single-phase transformerless photovoltaic inverters for leakage current suppression," *IEEE Trans. Ind. Electron.*, vol. 62, no. 7, pp. 4537–4551, Jul. 2015.
[10] S. Tan, H. Geng, G. Yang, and H. Wang, F. Blaabjerg, "Modeling framework of voltage-source converters based on equivalence with synchronous generator," *J. Modern Power Syst. Clean Energy*, vol. 6, no. 6, pp. 1291–1305, 2018.
[11] Y. Yang, F. Blaabjerg, and H. Wang, "Low-voltage ride-through of single-phase transformerless photovoltaic inverters," *IEEE Trans. Ind. Appl.*, vol. 50, no. 3, pp. 1942–1952, May/Jun. 2014.
[12] Y. Yang and F. Blaabjerg, "Overview of single-phase grid-connected photovoltaic systems," *Elect. Power Compon. Syst.*, vol. 43, no. 12, pp. 1352–1363, 2015.
[13] J. Wang, F. Luo, and Z. Ji, *et al.*, "An improved hybrid modulation method for the single phase H6 inverter with reactive power compensation," *IEEE Trans. Power Electron.*, vol. 33, no. 9, pp. 7674–7683, Sep. 2018.
[14] M. Islam, N. Afrin, and S. Mekhilef, "Efficient single phase transformerless inverter for grid-tied PVG system with reactive power control," *IEEE Trans. Sustain. Energy*, vol. 7, no. 3, pp. 1205–1215, Jul. 2016.
[15] T.-F. Wu, C.-L. Kuo, K.-H. Sun, and H.-C. Hsieh, "Combined unipolar and bipolar PWM for current distortion improvement during power compensation," *IEEE Trans. Power Electron.*, vol. 29, no. 4, pp. 1702–1709, Apr. 2014.
[16] T. Freddy, J. H. Lee, H. C. Moon, K. B. Lee, and N. Rahim, "Modulation technique for single phase transformerless photovoltaic inverters with reactive power capability," *IEEE Trans. Ind. Electron.*, vol. 64, no. 9, pp. 6989–6999, Sep. 2017.
[17] E. Afshari, G. Moradi, A. Ramyar, R. Rahimi, B. Farhangi, and S. Farhangi, "Reactive power generation for single-phase transformerless vehicle-to-grid inverters: A review and new solutions," in *Proc. IEEE Transp. Electrific. Conf. Expo.*, 2017, pp. 69–76.
[18] H. Qian, J. Zhang, J. -S Lai, and W. Yu, "A high-efficiency grid-tie battery energy storage system," *IEEE Trans. Power Electron.*, vol. 26, no. 3, pp. 886–896, Mar. 2011.
[19] C. Liu *et al.*, "Reliable transformerless battery energy storage systems based on cascade dual-boost/buck converters," *IET Power Electron.*, vol. 8, no. 9, pp. 1681–1689, Sep. 2015.
[20] B. Gu, J. Dominic, J.-S. Lai, C.-L. Chen, T. LaBella, and B. Chen, "High reliability and efficiency single-phase transformerless inverter for grid-connected photovoltaic systems," *IEEE Trans. Power Electron.*, vol. 28, no. 5, pp. 2235–2245, May 2013.
[21] C. Liu, Y. Wang, J. Cui, Y. Zhi, M. Liu, and G. Cai, "Transformerless photovoltaic inverter based on interleaving high-frequency legs having bidirectional capability," *IEEE Trans. Power Electron.*, vol. 31, no. 2, pp. 1131–1142, Feb. 2016.
[22] T. Ernö and M. Frisch, 2nd Generation of PFC Solutions. Available at: https://www.vincotech.com/support-and-documents/technical-library.html
[23] M. Frisch and T. Ernö, "High efficient topologies for next generation solar inverter," Available at: https://www.vincotech.com/support-and-documents/technical-library.html
[24] S. Aeaujo, P. Zacharias, and R. Mallwitz, "Highly efficient single-phase transformerless inverters for grid-connected photovoltaic systems," *IEEE Trans. Ind. Electron.*, vol. 57, no. 9, pp. 3118–3128, Sep. 2010.

[25] L. Huber, Y. Jang, and M. M. Jovanovic, "Performance evaluation of bridgeless PFC boost rectifiers," *IEEE Trans. Power Electron.*, vol. 23, no. 3, pp. 1381–1390, May 2008.
[26] J. Sun, "On the zero-crossing distortion in single-phase PFC converters," *IEEE Trans. Power Electron.*, vol. 19, no. 3, pp. 685–692, May 2004.
[27] J. Sun, "Input impedance analysis of single-phase PFC converters," *IEEE Trans. Power Electron.*, vol. 20, no. 2, pp. 308–314, Mar. 2005.
[28] B. Liu, M. Su, J. Yang, D. Song, D. He, and S. Song, "Combined reactive power injection modulation and grid current distortion improvement approach for H6 transformer-less photovoltaic inverter," *IEEE Trans. Energy Convers.*, vol. 32, no. 4, pp. 1456–1467, Dec. 2017.
[29] P. Sun, C. Liu, J. S. Lai, and C. L. Chen, "Cascade dual buck inverter with phase-shift control," *IEEE Trans. Power Electron.*, vol. 27, no. 4, pp. 2067–2077, Apr. 2012.

Jianhua Wang (M'11) received the B.S. and Ph.D. degrees in electrical engineering from Nanjing University of Aeronautics & Astronautics, Nanjing, China, in 2004 and 2010, respectively.

In 2010, he joined the Faculty of School of Electrical Engineering, Southeast University, Nanjing, China, where he is currently an Associate Research Professor. He has authored or coauthored more than 40 technical papers. He is the holder of three China patents. His main research interests include MVdc, solid-state transformer, power electronics system stability, distributed generation, and micro-grid.

Shang Gao received the B.S. degree from Shandong University, Jinan, China, in 2017, and currently working toward the M.S. degree at Southeast University, Nanjing, China.

His main research interests include MVdc and power electronics system stability.

Yichao Sun (S'13–M'17) received the B.S. and Ph.D. degrees in electrical engineering from Southeast University, Nanjing, China, in 2010 and 2017, respectively.

From February 2015 to August 2016, he was a Visiting Scholar with the Power Electronics Group, RMIT University, Melbourne, Vic., Australia. Since 2017, he joined the School of Electrical and Automation Engineering, Nanjing Normal University, Nanjing, China, where he is currently a Lecturer. His current research interests include the modulation and control of power electronic converters, with a particular emphasis on multilevel converters.

Zhendong Ji received the B.S. and Ph.D. degrees in electrical engineering from Southeast University, Nanjing, China, in 2007 and 2015, respectively.

Since 2015, he joined the School of Automation, Nanjing University of Science and Technology, Nanjing, China, where he is currently a Lecturer. His main research interests include cascade multilevel converters and solid-state transformers.

Lexiang Cheng received the B.S. degree from Nanjing university of Science and Technology, Nanjing, China, in 2007, and the M.E. degree from Southeast University, Nanjing, China, in 2010.

Since 2010, he joined State Grid Nanjing Power Supply Company, Nanjing, China. His main research interests include integration techniques of distributed generation and renewable energy sources.

Lingyu Li received the B.S. degree in applied physics from Hohai University, Nanjing, China, in 2008, and the M.S. degree in electrical engineering from Southeast University, Nanjing, China, in 2016.

Since 2016, she joined in State Grid Yancheng Power Supply Company, Yancheng, China, where she is currently an Electrical Engineer. Her main research interests include distributed generation and substation operation and maintenance.

Wei Gu (M'06–SM'16) received the B.S. and Ph.D. degrees in electrical engineering from Southeast University, Nanjing, China, in 2001 and 2006, respectively.

From 2009 to 2010, he was a Visiting Scholar with the Department of Electrical Engineering, Arizona State University, Tempe, AZ, USA. He is currently a Professor with the School of Electrical Engineering, Southeast University. He is the Director of the Institute of Distributed Generations and Active Distribution Networks. His research interests include distributed generations and microgrids and active distribution networks.

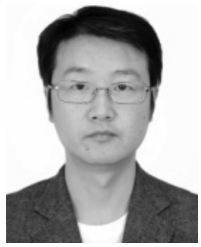

Jianfeng Zhao received the B.S. degree from Huainan Mining Institute, Huainan, China, the M.S. degree from Nanjing University of Aeronautics & Astronautics, Nanjing, China, and the Ph.D. degrees from Southeast University, Nanjing, China, in 1995, 1998, and 2001, respectively, all in electrical engineering.

In 2001, he joined the Faculty of School of Electrical Engineering, Southeast University, where since 2008 he has been a Professor and has been engaged in teaching and research in the field of high-power power electronics. Since 2014, he has also been the Dean of School of Electrical Engineering, Southeast University. He has authored or coauthored more than 100 technical papers. He holds more than 50 China patents. His current research interests include utility applications of power electronics in smart grid such as solid-state transformer, active filters for power conditioning, flexible ac-transmission system devices, multilevel ac-motor drives, and efficient energy utilization.